applied sciences

MDPI

Article

Multi-Mode Compound Grasping Robot Finger Driven by Linkage

Yinkai Dong [1] and Wenzeng Zhang [2,*]

[1] Department of Mechanical and Energy Engineering, Southern University of Science and Technology, Shenzhen 518055, China; yinkai@mit.edu
[2] Robotics Lab., X Institute, Shenzhen 518038, China
* Correspondence: zhangwenzeng.1994@tsinghua.org.cn

Abstract: The current underactuated robot hands use a single actuator to drive multiple degrees of freedom, enabling them to perform grasping functions. This paper design a multi-mode compound grasping robot finger driven by linkage, called MCG hand. The MCG hand includes a base, two motors, three phalanx, multiple shafts, two motors, two driving wheels, four linkages, three springs, and two limit blocks. This unique design allows the MCG finger to perform various grasping modes, such as parallel, coupling, middle, and distal phalanx self-adaptive, proximal, and distal gesture-changeable modes, as well as their combinations. The device can independently control the rotation of the proximal phalanx and the distal joint and realize the parallel pinching action of the distal phalanx. It can also realize the coupling function of the proximal and distal phalanx. It has automatic adaptability to objects of different shapes and sizes. Furthermore, the MCG finger provides enveloping grasping with multiple contact points, resulting in a more stable grip. The easy switching between modes through simple control, along with its wide application range and low manufacturing and maintenance costs, make the MCG hand a versatile solution for various applications.

Keywords: robot hand; multi grasping modes; coupling grasping; self-adaptive grasping; gesture-changeable grasping; underactuated finger

Citation: Dong, Y.; Zhang, W. Multi-Mode Compound Grasping Robot Finger Driven by Linkage. *Appl. Sci.* **2023**, *13*, 5550. https://doi.org/10.3390/app13095550

Academic Editor: Alessandro Gasparetto

Received: 31 March 2023
Revised: 20 April 2023
Accepted: 25 April 2023
Published: 29 April 2023

1. Introduction

The development of robotic hands that closely resemble the biological and kinematic characteristics of the human hand has been a long-standing challenge [1,2]. Humanoid dexterous hands, which can perform various grasping and manipulation tasks, often require a separate motor for each joint, resulting in significant challenges related to sensing, control, and high costs. The delicate and precise DLR hand [3,4], the non-anthropomorphic Goldfinger [5], and the highly versatile GIFU hand [6,7], can make them difficult to design, build, and maintain. The challenges in controlling dexterous hands are exemplified by studies that address the need for optimization techniques for motion control trajectories [8], highlighting the sophisticated sensing and control algorithms required to coordinate movements effectively. To overcome these limitations, researchers have been motivated to explore alternative approaches.

Underactuated robot hands have attracted attention for their ability to provide a wide range of grasping capabilities and higher output force with fewer motors and more joint degrees of freedom. Laliberté and Gosselin introduced the design of two-degree-of-freedom underactuated fingers, which demonstrated reduced complexity, lower cost, and improved performance [9,10]. This innovative design has garnered significant attention in the field of robotics, as evidenced by subsequent research on underactuated hands. Laliberte et al. [11] provides a comprehensive overview of under-actuation in robotic grasping hands, and Dollar and Howe [12] present a study on joint coupling design for underactuated grippers. Recent advances in simulation tools, such as the work by Bencak, Hercog, and Lerher,

focus on improving the efficiency and reliability of robotic grasping through pick-point evaluation for a 2-F robotic gripper [13].

Underactuated fingers, including parallel (PA), coupling (CO), and self-adaptive (SA) grasping fingers, have been developed to address the limitations of dexterous hands. The distal phalanx of the parallel grasping finger always keeps the original posture relative to the base when it moves, which is suitable for grabbing objects placed on a plane. When the coupling grasping finger is leaning towards the object, all phalanxes rotate simultaneously, and the speed ratio of the second phalanx to the first phalanx is a scalar greater than 1. The coupling grasping finger is suitable for holding objects with the distal phalanx on the desktop.

Self-adaptive grasping mechanisms allow robots to grasp objects of various shapes and sizes with minimal input from the control system. When actuating the self-adaptive finger, the proximal phalanx rotates, and the distal phalanx does not constantly rotate to the proximal phalanx. When the proximal phalanx contacts the object and is blocked, the distal phalanx continues to rotate automatically, which adapts to the different shapes and sizes of the object and achieves the envelope grasping effect [14,15]. The self-adaptive grasping mode benefits from synchronized finger and wrist movements, which can improve the grasp success rates and mitigate object slippage during hand closure [16]. This can also be achieved by using soft materials [17] and pneumatic or hydraulic actuation [18]. The soft–rigid tendon-driven grippers investigated in [19] allow robots to grasp objects of various shapes and sizes with minimal input from the control system. These adaptive mechanisms have shown promise for improving grasp stability and versatility [20]. However, only the proximal phalanx is driven before grasping, and the distal phalanx does not have a grasping motion. The limited range of motion of the distal phalanx in self-adaptive fingers constrains their overall grasping capabilities.

To overcome these drawbacks, researchers have focused on developing compound grasping modes that combine the strengths of parallel, coupling, and self-adaptive fingers.

The integration of coupling and self-adaptive grasping mechanisms leads to the development of the coupling adaptive composite grasping mode (COSA mode) [12]. Matrone et al. [21] present a study on real-time myoelectric control of multi-fingered hand prostheses using principal component analysis, hybrid flexible robotic gripper mechanism presented by [22] allows for improved grasping capabilities, including the implementation of a power grip through the sequential movement of the rigid link and the flexible mechanism. This mode allows the robotic hand to initially adopt a coupling motion, where both joints rotate in the same direction, and the distal phalanx rotates faster than the proximal phalanx. Upon contact with the object, the hand automatically switches to the self-adaptive grasping mode, enabling the distal phalanx to rotate until it touches the object. This results in a more anthropomorphic and stable grasp, increased grasping efficiency, and more reasonable force distribution [23,24].

This mechanism has been extensively studied and developed by researchers, leading to several publications such as the COSA-FBA hand with five-gear mechanisms and built-in actuators [25], and the COSA-LET finger with a linear empty-trip transmission [26]. Applications of the COSA finger in humanoid robotic hands have demonstrated its potential to improve grasping performance [27,28].

Similarly, the parallel self-adaptive grasping mode (PASA mode) combines the strengths of parallel and self-adaptive grasping mechanisms. A single-actuator gripper utilizing a crawler on the fingertip is proposed, enabling the lifting of thin objects and transitioning between grasp modes passively [29]. Ref. [30] introduces a parallel and self-adaptive underactuated finger with novel belt and cam-link mechanisms. The Velo gripper [31] demonstrates the ability to perform parallel, enveloping, and fingertip grasps using single active tendon actuation and passive adaptation for increased versatility. In this mode, the robotic hand initially adopts a parallel grasping motion, maintaining the posture of the distal phalanx relative to the base. Upon contact with the object, the hand automatically switches to the self-adaptive grasping mode, enhancing the practicability and versatility of the finger [32].

Changing the initial position of each finger joint during grasping is called gesture-changeable [33,34]. The gesture changeable grasping mode includes self-adaptive grasping and pre-bending action functions. Before grasping the object, the mechanism can flexibly adjust the ready posture (initial configuration) of the finger to hold the object according to the size and shape of the object.

The second motor is added to the self-adaptive underactuated finger to obtain more dexterity. This kind of finger adds the function of flexible changing position to the original self-adaptive underactuated finger, forming a more dexterous underactuated finger.

Traditional robotic hands face challenges due to their complexity, sensing, control, and high costs. Underactuated fingers, such as parallel, coupling, and self-adaptive fingers, have been developed to address these limitations but still exhibit constraints in grasping capabilities. To overcome these issues, this paper introduces a novel multi-mode compound grasping robot finger driven by linkage (MCG finger), capable of performing six distinct grasping modes, including parallel (PA), coupling (CO), middle phalanx self-adaptive (M-SA), distal phalanx self-adaptive (D-SA), proximal gesture-changeable (P-GC), and distal gesture-changeable (D-GC), as well as their combinations. The MCG finger addresses the challenges faced by traditional dexterous hands by offering a versatile and adaptable solution with reduced complexity and cost.

With its versatile range of motion, the MCG finger has a wide range of potential applications in industrial manufacturing [35], hand rehabilitation [36], medical treatment [37,38], military robots [39], and other scientific fields. The importance of selecting the appropriate gripper for a robotic manipulator, as it directly influences the efficiency and performance of the system, is emphasized by the comprehensive review of various gripper classifications and their applications provided in the work of [40]. This paper presents the design concept, working principle, and concrete structure, as well as dynamic and kinematic analyses of the MCG finger [41], making a contribution to the field by offering a novel and efficient solution for robotic grasping.

2. Design of MCG Finger

2.1. Design Concept

The PA, CO, M-SA, D-SA, P-GC, and D-GC modes are six basic grasping types for the MCG fingers.

2.1.1. Paralleling Grasping Mode (PA Mode)

Paralleling grasping means that when grasping the object, the proximal phalanx rotates positively, and the distal phalanx rotates negatively at the same angle, which keeps the posture of the distal phalanx unchanged relative to the base. As shown in Figure 1a.

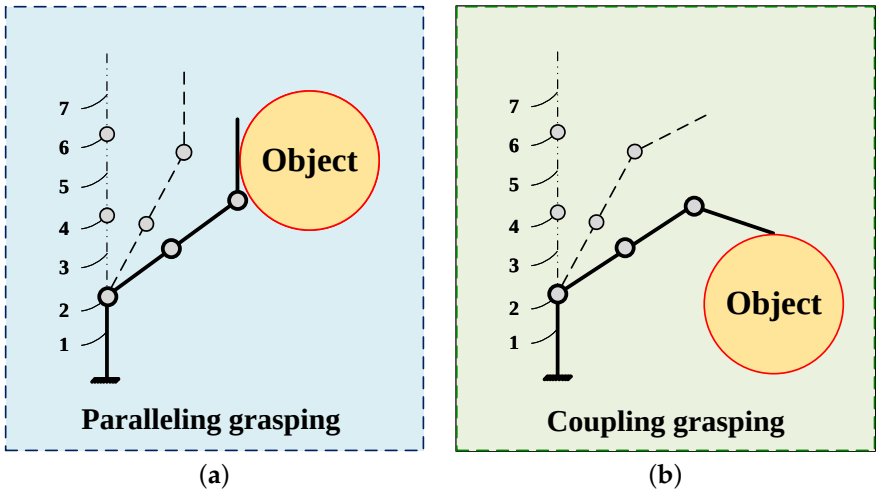

Figure 1. (**a**) The PA grasping mode and (**b**) the CO grasping mode. 1-Base; 2-Proximal shaft; 3-Proximal phalanx; 4-Middle shaft; 5-Middle phalanx; 6-Distal shaft; 7-Distal phalanx.

2.1.2. Coupling Grasping Mode (CO mode)

The coupling grasping mode is tailored for objects with tapered or conical geometries. In this mode, the distal phalanx rotates in the same direction and at a proportional rate as the proximal phalanx, which adapts to the object's shape and minimizes slippage during handling, as shown in Figure 1b.

2.1.3. Middle Phalanx Self-Adaptive Grasping Mode (M-SA Mode)

Middle phalanx self-adaptive grasping is a mode of grasping where the middle finger joint can adjust to the shape of irregularly shaped objects. In M-SA grasping, the middle phalanx rotates independently from the proximal phalanx and passively rotates in response to the movement of the distal phalanx. This helps the finger to conform to the shape of the object, which results in a more stable and secure grip on objects with varying curvatures. M-SA grasping is particularly useful for grasping objects with irregular surfaces, as it allows the finger to adapt to the object's shape more effectively, as shown in Figure 2a.

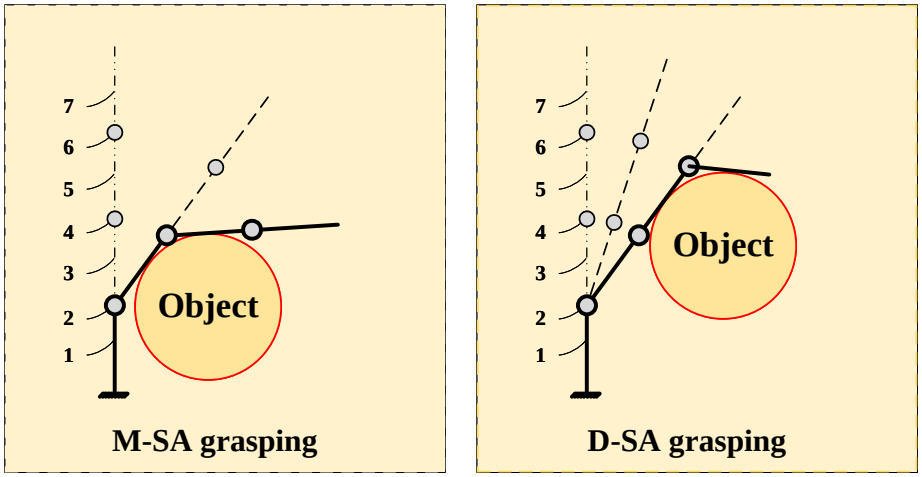

(**a**) (**b**)

Figure 2. (**a**) The M-SA grasping mode and (**b**) the P-SA grasping mode.

2.1.4. Distal Phalanx Self-Adaptive Grasping Mode (D-SA Mode)

Distal phalanx self-adaptive grasping involves the passive rotation of the finger's distal phalanx until it comes into contact with the object. This gripping mode is only activated after the proximal and middle phalanges have been fixed in position. The D-SA mode of grasping is particularly well-suited for gripping objects with small protrusions or irregularities at their distal end. This is because the distal phalanx continues to rotate until it contacts the object, thereby providing a self-adaptive envelope-grasping function. This unique gripping mechanism allows the MCG finger to securely grip objects with complex geometries, providing an efficient and effective way to handle such objects, as shown in Figure 2b.

2.1.5. Proximal Gesture-Changeable Grasping Mode (P-GC Mode)

Proximal gesture-changeable grasping allows the finger to adjust its proximal phalanx position during grasping by controlling the two actuators' speed. This versatility enables the finger to handle objects with varying thicknesses or adjust the grip during manipulation, ensuring a stable and secure hold regardless of the grasping mode used, as shown in Figure 3a.

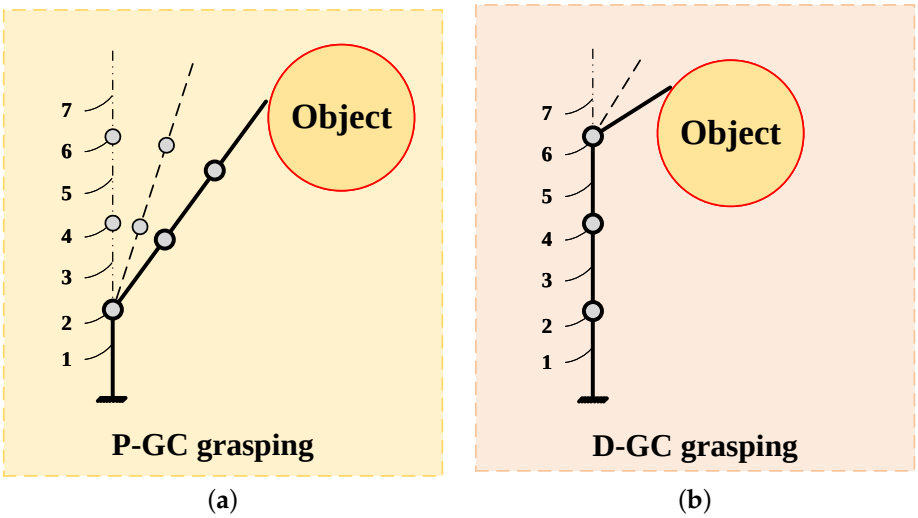

Figure 3. (**a**) The P-GC grasping mode and (**b**) the D-GC grasping mode.

2.1.6. Distal Gesture-Changeable Grasping Mode (D-GC Mode)

Distal gesture-changeable grasping allows for independent adjustment of the distal phalanx during the grasping process while keeping the proximal and middle phalanges unchanged. This mode is suitable for handling objects that require precise positioning of the distal phalanx or objects with uneven surfaces where the distal phalanx needs to be adjusted for a stable grip, as shown in Figure 3b.

As to the design concept of the MCG finger, six grasping modes are fused to improve the grasping performance. Through the combination of these six grasping modes, a variety of composite grasping modes can be obtained, such as PA-M&D-SA grasping mode and CO-M&D-SA grasping mode(shown in Figures 4 and 5, which is suitable for flexible application in multiple environments. Different grasping modes can be switched by controlling the speed of rotation and the rotation and stop of the two motors. Various composite grasping modes broaden the application fields of MCG fingers, which can be widely used in industrial manufacturing, hazardous environment operation, marine resources detection, and other scientific fields.

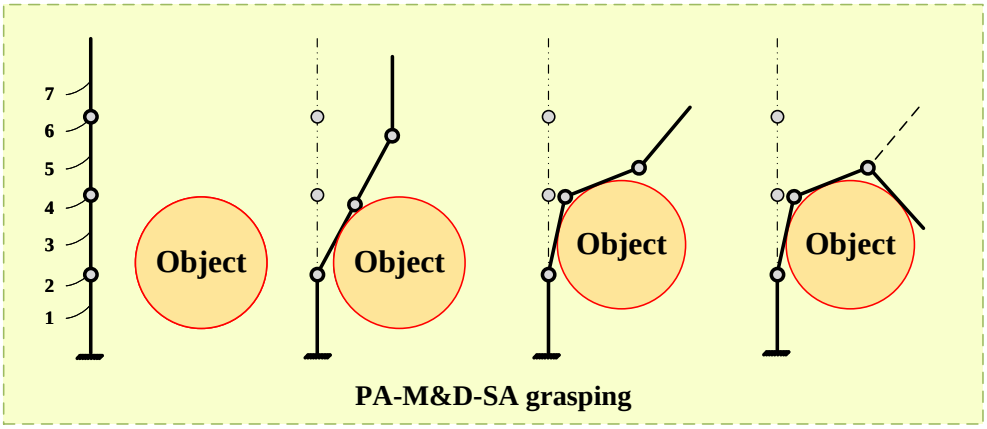

Figure 4. The PA-M&D-SA grasping mode.

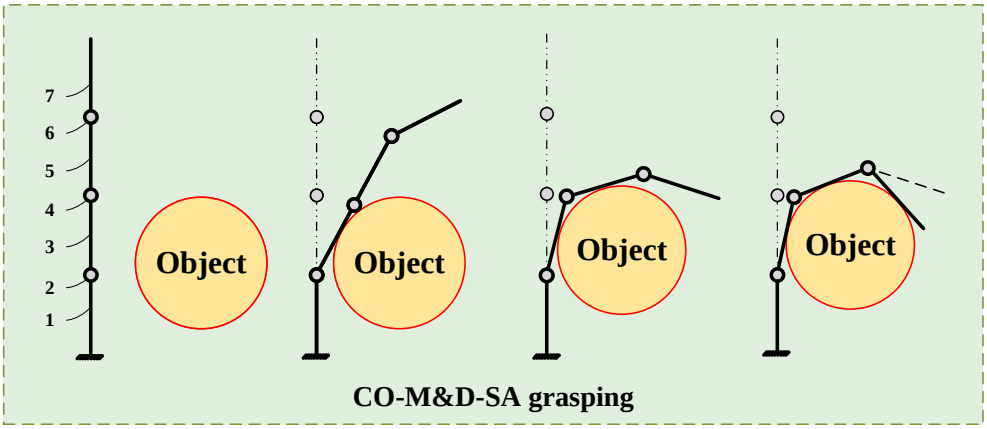

Figure 5. The CO-M&D-SA grasping mode.

2.2. Structure of MCG Finger

According to the design concept, the MCG finger combines six grasping modes and achieves a variety of grasping effects through the joint driving of two motors. The detailed structure is shown in the 3D assembly model shown in Figures 6 and 7.

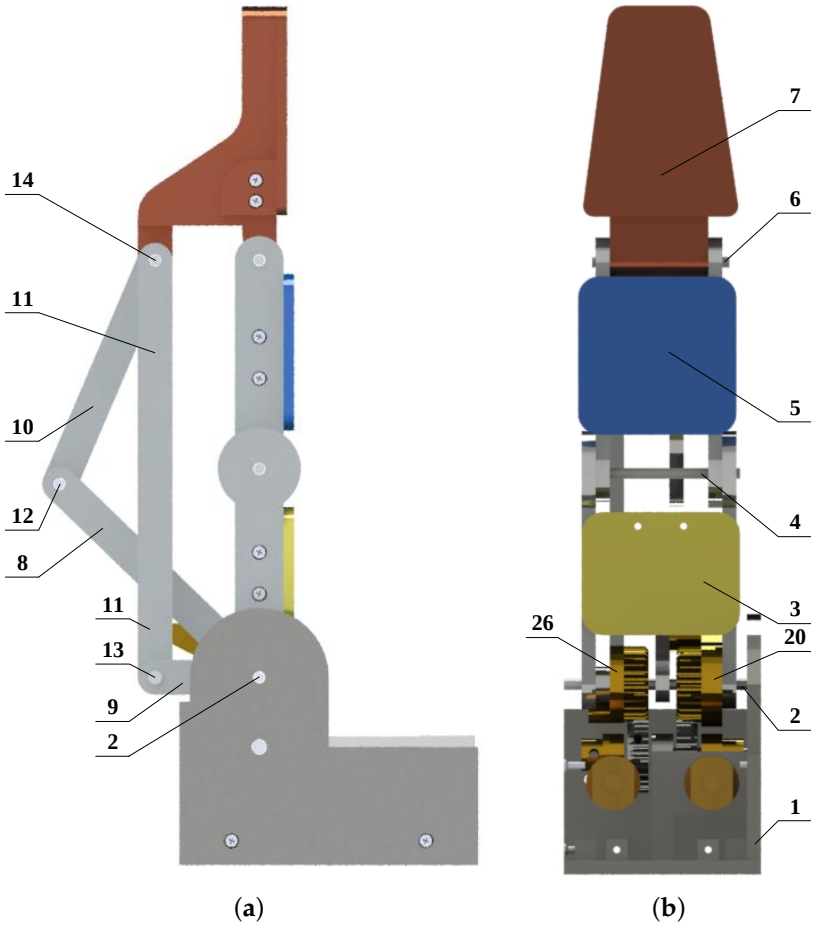

Figure 6. (**a**) Side view and (**b**) front view of the MCG finger. 1-Base; 2-Proximal shaft; 3-Proximal phalanx; 4-Middle shaft; 5-Middle phalanx; 6-Distal shaft; 7-Distal phalanx; 8-11-1st-4th linkage; 12-14-1st-3rd shaft; 15-1st motor; 16-1st reducer; 17-1st worm; 18-1st worm gear; 19-1st gear; 20-1st driving gear; 21-2nd motor; 22-2nd reducer; 23-2nd worm; 24-2nd worm gear; 25-2nd gear; 26-2nd driving gear; 27-28-1st-2nd pushing block; 29-31-1st-3rd spring; 32-33-1st-2nd limit block. All the numbers in the following figures represent the same component of the MCG finger.

The MCG finger comprises the base, proximal phalanx, middle phalanx, distal phalanx, proximal shaft, middle shaft, distal shaft, the first to the third shaft, the first to the fourth linkage, the first and second transmission mechanism, the first and second driving wheel, the first and second pushing block, the first to third spring piece, the first and second limiting block. The center lines of the proximal shaft, middle shaft, distal shaft, and first to third shaft are parallel to each other.

To simplify the description, set the center points of the proximal shaft, middle shaft, distal shaft, and first to the third shaft as A, B, C, G, E, F; set the end point of the distal phalanx as D. The second linkage AE has equal length as CF. The sum of the lengths of the proximal phalanx AB and the middle phalanx BC is equal to the length of the fourth linkage EF, as shown in Figure 8.

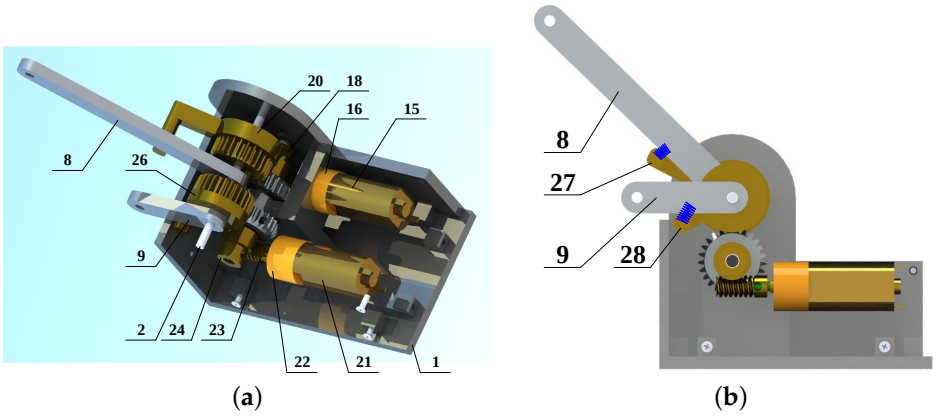

Figure 7. Oblique view (**a**) and main view (**b**) of inner parts of MCG finger.

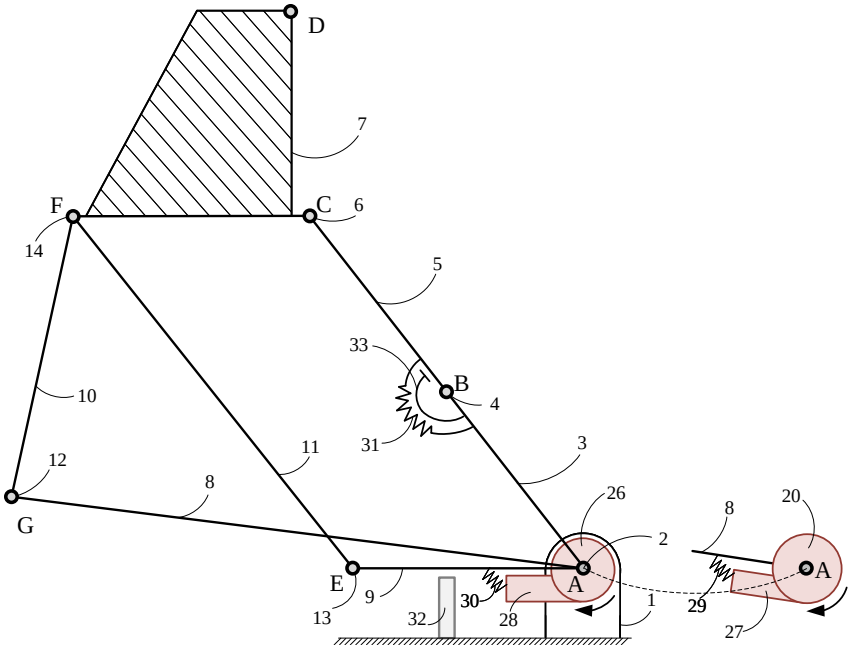

Figure 8. Structure sketch of the MCG finger.

2.3. Working Principle of MCG Finger

In its initial state, the MCG finger is set up so that the first linkage makes contact with the first pushing block, the second linkage contacts the first limiting block, and the middle phalanx connects with the second limiting block, thanks to the force exerted by the first to the third springs. By coordinating the movement of the two motors, the MCG finger can switch between various composite grasping modes.

During the initial stage, the first, second, and third springs will pre-stretch and create a contact angle ξ_{1-3} between the first linkage and the first pushing block, the second linkage and the first limiting block, and the middle phalanx and the second limiting block, respectively. As the first and second pushing blocks are connected to the first and second motors, respectively, this ensures that the MCG finger remains in a stable state prior to grasping.

According to the structure of the MCG finger, the working principle is as follows (shown in Figures 9 and 10):

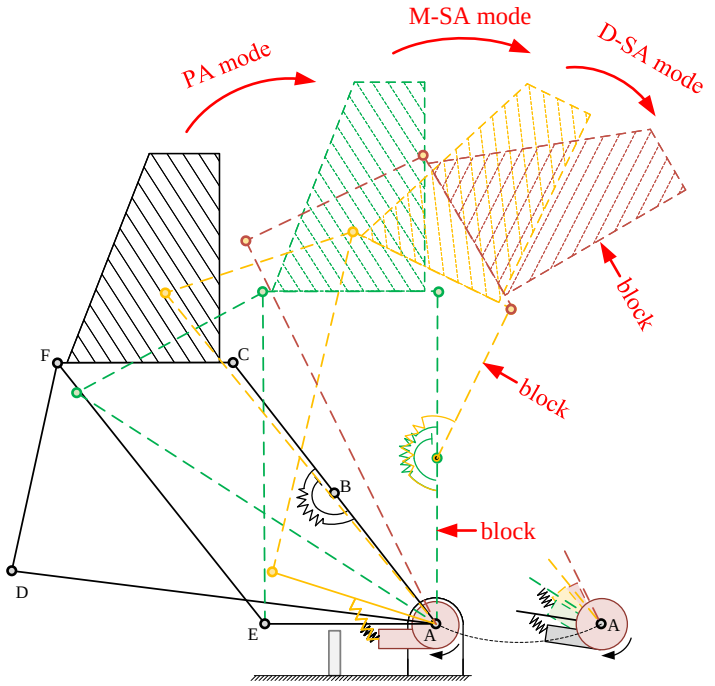

Figure 9. Working principle of the MCG finger (PA-S&D-SA mode).

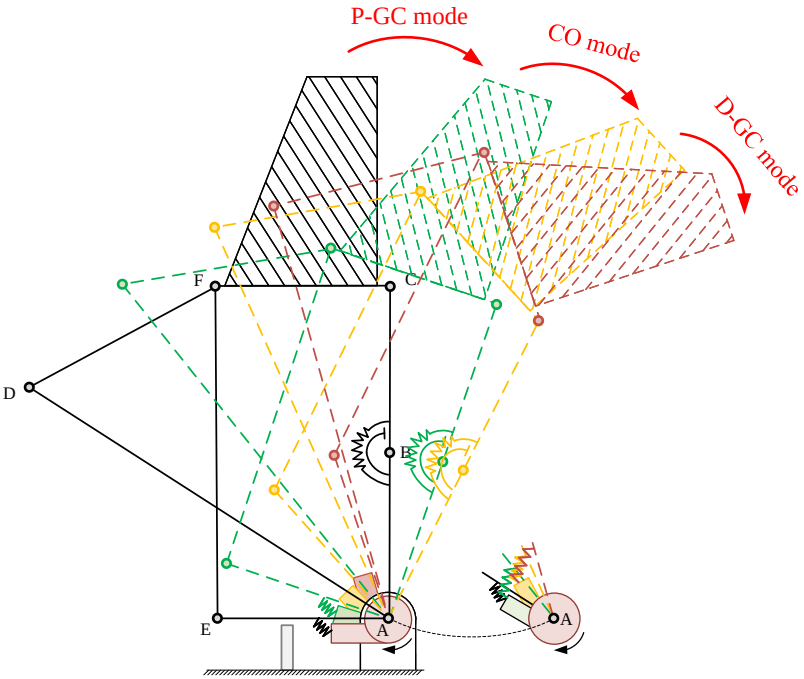

Figure 10. Working principle of the MCG finger (P-GC, CO and D-GC mode).

One of the characteristics of underactuated robot fingers is that they can grasp without complicated control. Therefore, when controlling the movement of MCG fingers, each motor will have three different output states: stop (speed is zero), rotate(speed is $0.5v$), and rotate(speed is v). v is the speed of the motor at rated voltage, and correspondingly, $0.5v$ is the speed at half of the given rated voltage. For different grasping modes, different output speeds can be set for the two motors; details can be seen in the graph, which is shown in Table 1.

Table 1. The state and the speed of the two motors.

Mode	STATE 1	SPEED 1	STATE 2	SPEED 2
PA	R [*1]	v [*3]	S [*2]	0
CO	R	$0.5v$	R	v
P-GC	R	v	R	v
D-GC	S	0	R	v
M-SA	R & S	v & 0	R & S	v & 0
D-SA	R & S	v & 0	R & S	v & 0

[*1] R represent rotate. [*2] S represent stop. [*3] v is a constant speed.

In order to effectively switch between different grasping modes, the MCG finger relies on the contact conditions with the object and the desired outcome during the grasping process. For active modes (PA, CO, P-GC, and D-GC grasping modes), the MCG finger proactively adjusts its position and movement based on predefined commands, which are determined by the object's shape and the desired grip. On the other hand, the passive modes (M-SA and D-SA) are activated in response to contact with the object, allowing the finger to adapt to the object's shape for a more stable and secure grip. The contact points and the sequence in which the phalanges interact with the object determine the appropriate grasping mode. As the MCG finger encounters an object, the contact conditions are evaluated in real-time, allowing the system to adapt and choose the most suitable grasping mode.

The specific grasping process is shown below (take the PA-M&D-SA mode, for example):

The first motor rotates forward at speed v, drives the first worm through the first reducer, the first worm wheel rotates, and the first transition shaft rotates to drive the first gear to rotate so that the first transmission wheel rotates forward, and the first pushing block rotates forward, pushing the first linkage to rotate around the proximal shaft, and then pushing the distal phalanx through the third linkage.

Because the second motor is not started, the second driving wheel and the second pushing block are not moved. The second spring connects the second linkage with the second pushing block, which makes the second linkage maintain the initial posture relative to the base. Before the proximal phalanx and the middle phalanx do not contact the object, the quadrilateral ACFE maintains the parallelogram, so the phalanx FC remains parallel to the phalanx AE, that is, the distal phalanx keeps the initial posture unchanged relative to the base. Thus, the parallel clamping process is realized.

When contacting objects, there are three possible results:

1. The distal phalanx first contacts the object, the grasping is finished, and the parallel clamping function for the object is realized.
2. The middle phalanx first contacts the object, and it will be blocked. Then the first motor will continue to rotate. The first linkage will push the distal phalanx to rotate around the distal shaft until the distal phalanx touches the object, which is the distal self-adaptive grasping mode. At the same time, since the second motor does not rotate, the second linkage will leave the second pushing block, and the second spring will be stretched.
3. The distal phalanx first contacts the object, and it will be blocked. The MCG finger will automatically switch to the middle phalanx self-adaptive grasping mode. The movement of the first motor will continue to push the distal and middle phalanxes to

move forward, which will make the second phalanx overcome the pre-bending force between it and the second limit block and rotate around the middle shaft. After the middle phalanx touches the object, the MCG will perform D-SA mode.

The movement process of the other grasping modes of the MCG finger is similar to the PA-M&D-SA mode, so it will not be repeated here.

Importantly, there is an interference problem when driving the first motor and the second motor at different speeds. For example, in the distal self-adaptive grasping stage, the first motor continues to rotate, and its impact on the second linkage is greater than that of the second motor, which will make the second linkage overcome the pull of the second spring and leave the second pushing block. Similarly, in the distal phalanx gesture-changeable grasping mode, only the second motor rotates at speed v. The rotation of the distal phalanx will also make the first linkage overcome the tension of the first spring and leave the first pushing block. Compared with the direct driving of two different linkages, the driving system of pushing block, spring, and linkage is more effective in improving the switching stability between different modes.

3. Mechanical Analysis and Simulation

In this section, we will discuss the parameters that affect MCG fingers in detail. The kinematic and dynamic model of the MCG finger is shown in Figure 11. The grasping force of the MCG finger when grasping an object is analyzed to evaluate the stability of grasping. The simulation results are given by MATLAB, which shows the grasping function of the MCG hand.

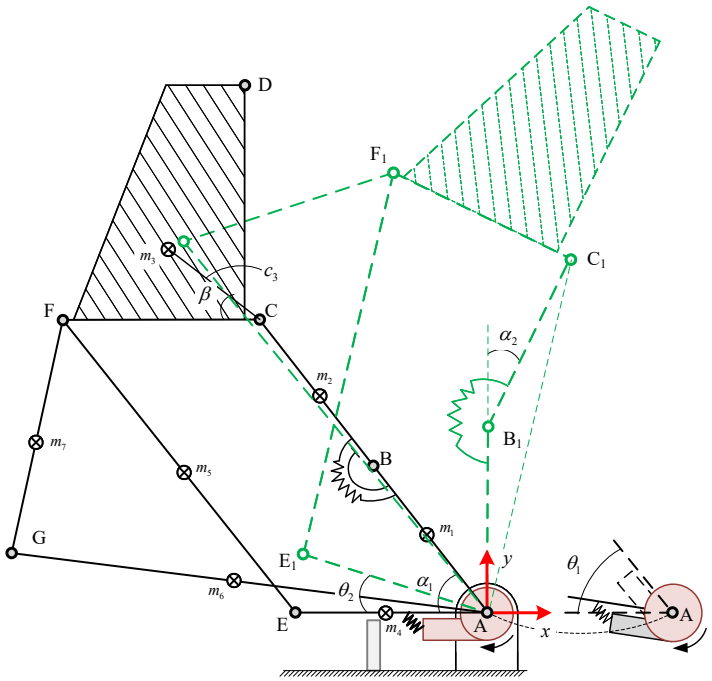

Figure 11. Kinematic and dynamic model of the MCG finger.

θ_1—Angle of the first linkage concerning the base, which is the angle between AG and the negative direction of the x-axis, rad;

θ_2—Angle of the second linkage concerning base, which is the angle between AE and the negative direction of the x-axis, rad;

α_1—Rotational angle of the transition shaft, which is the angle between AB and the negative direction of the x-axis, rad;

α_2—Angle of the first phalanx concerning the second phalanx, which is the angle between AB and BC, rad;

m_{1-7}—Mass of the proximal, middle, and distal phalanx, second, fourth, first, and third linkage, respectively, kg;

l_{1-7}—Length of AB, BC, CD, AE, EF, AG, and GF, respectively, m.

β—The angle between the line from the distal shaft to the centroid of the distal phalanx and the line CF in the distal phalanx, rad.

k_{1-3}—Torsion coefficient of the first, second, and third spring, respectively, N/rad.

ξ_{1-3}—The pre-rotation angle of the first, second, and third spring, respectively, rad.

τ_{1-2}—The torque applied by the first motor, and the second motor, respectively, N/rad.

The MCG finger controls three degrees of freedom through two actuators, which is an underactuated system. In the simulation analysis of the MCG finger, it is found that when the first and second links are driven to control the motion of the MCG finger, the simulation results are extremely complex. This is because the torque exerted by the first driver on the first linkage acts on the first phalanx and the second phalanx comprehensively, so the solution is more complex. To simplify the simulation while obtaining the kinematics and dynamics analysis of the MCG finger, this paper chooses to place the first and second virtual drivers at the proximal and middle joint axes, respectively, to equivalently replace the effect of the first motor on the proximal and middle phalanx. In real motion, the kinematics curve of the first driver can be inversely solved by using the motion angle of two virtual motors during simulation. If the parameters of the first driver solved are used as input, the results equivalent to the simulation can be obtained.

Take point A (Proximal shaft) as the origin; the horizontal direction is the x-axis, the vertical direction is the y-axis, and the vertical point A outward is the z-axis to establish the coordinate system as shown in Figure 11. The coordinate of point A can be obtained directly:

$$\mathbf{r_A} = [0 \quad 0 \quad 0] \tag{1}$$

The length of AB (proximal phalanx) is l_1, the angle between AB and the negative direction of the x-axis is α_1, so the coordinate of B is:

$$\mathbf{r_B} = [-l_1 \cos(\alpha_1) \quad l_1 \sin(\alpha_1) \quad 0] \tag{2}$$

The length of BC (proximal phalanx) is l_2, the angle between AB and BC is α_2, the calculated coordinate of B can be obtained:

$$\mathbf{r_C} = [-l_2 \cos(\alpha_1 + \alpha_2) - l_1 \cos(\alpha_1) \quad l_2 \sin(\alpha_1 + \alpha_2) + l_1 \sin(\alpha_1) \quad 0] \tag{3}$$

The length of AE (second linkage) is l_2, the angle between AB and BC is θ_2, the coordinate of E can be obtained:

$$\mathbf{r_E} = [-l_4 \cos(\theta_1) \quad l_4 \sin(\theta_1) \quad 0] \tag{4}$$

The parameters of the MCG finger are mainly determined by the second driver and the first and second virtual drives. Therefore, after the coordinates of points A, B, C, and E are determined, the parametric coordinates of all linkage positions of the MCG finger can be solved by the geometric method. The coordinates of the solved D, F, and G points are complex and will not be shown here. In this paper, they will be expressed by $\mathbf{r}_D$, $\mathbf{r}_F$, $\mathbf{r}_G$, respectively.

3.1. Statistics Analysis of MCG Finger

Through static analysis, we can obtain the response of MCG finger structure under a given static load. Given the angle of the first and second linkages and the input torque of the first motor acting on each linkage, respectively, we can derive the output force of the proximal, middle, and distal phalanx under this condition. Through the simulation results, we can judge the grasping effect of each grasping mode by analyzing the stress state of each phalanx.

Since we have obtained the coordinates of each key point of the MCG finger, the unit vector of each linkage can also be obtained.

$$\widehat{\mathbf{e}}_{AB} = (\mathbf{r}_B - \mathbf{r}_A)/l_1 \tag{5}$$

$$\widehat{\mathbf{e}}_{BC} = (\mathbf{r}_C - \mathbf{r}_B)/l_2 \tag{6}$$

$$\widehat{\mathbf{e}}_{AE} = (\mathbf{r}_E - \mathbf{r}_A)/l_4 \tag{7}$$

$$\widehat{\mathbf{e}}_{FC} = (\mathbf{r}_C - \mathbf{r}_F)/l_4 \tag{8}$$

$$\widehat{\mathbf{e}}_{EF} = (\mathbf{r}_F - \mathbf{r}_E)/l_5 \tag{9}$$

$$\widehat{\mathbf{e}}_{AG} = (\mathbf{r}_G - \mathbf{r}_A)/l_6 \tag{10}$$

$$\widehat{\mathbf{e}}_{GF} = (\mathbf{r}_F - \mathbf{r}_G)/l_7 \tag{11}$$

The first linkage and the first pushing block are connected by the first spring. Initially, the first spring has a pre-rotating angle ξ_1, which will make them closely connected. The output torque of the first motor is τ_1, which acts on the first linkage through the first pushing block. The force of this moment acting on point G is:

$$\mathbf{F}_G = \tau_1/l_6 \cdot \mathbf{R}_{z,-90^\circ} \cdot \widehat{\mathbf{e}}_{AG} \tag{12}$$

where $\mathbf{R}_{z,-90^\circ}$ is the rotation matrix of -90 degrees around the z-axis (the angle of counter-clockwise rotation is positive).

The angle η_1 between $\mathbf{F}_G$ and $\widehat{\mathbf{e}}_{GF}$ is:

$$\eta_1 = \cos^{-1}\left(\frac{{\mathbf{F}_G}^T \cdot \widehat{\mathbf{e}}_{GF}}{\|\mathbf{F}_G\| \cdot \|\widehat{\mathbf{e}}_{GF}\|}\right) \tag{13}$$

The force at point G acts on point F through the third linkage:

$$\mathbf{F}_{F,\tau_1} = \frac{{\mathbf{F}_G}^T \cdot \widehat{\mathbf{e}}_{GF} \cdot \widehat{\mathbf{e}}_{GF}}{\cos^2(\eta_1)} \tag{14}$$

The torque output by the second motor acts on the second linkage. In the initial state, the second linkage maintains contact with the second pushing block under the action of the second spring, and the pre-rotation angle of the second spring is assumed to be ξ_2. The spring will have an impedance effect on the output of the second motor, so the force at point E is:

$$\mathbf{F}_E = \tau_2/l_4 \cdot \mathbf{R}_{z,-90^\circ} \cdot \widehat{\mathbf{e}}_{AE} \tag{15}$$

Similar to $\mathbf{F}_G$, The angle η_2 between $\mathbf{F}_E$ and $\widehat{\mathbf{e}}_{EF}$ and the force at point E acts on point F through the forth linkage are:

$$\eta_2 = \cos^{-1}\left(\frac{{\mathbf{F}_E}^T \cdot \widehat{\mathbf{e}}_{EF}}{\|\mathbf{F}_E\| \cdot \|\widehat{\mathbf{e}}_{EF}\|}\right) \tag{16}$$

$$\mathbf{F}_{F,\tau_2} = \frac{{\mathbf{F}_E}^T \cdot \widehat{\mathbf{e}}_{EF} \cdot \widehat{\mathbf{e}}_{EF}}{\cos^2(\eta_2)} \tag{17}$$

Combining the output torque of the two motors, the resultant force at point F is:

$$\mathbf{F}_F = \mathbf{F}_{F,\tau_1} + \mathbf{F}_{F,\tau_2} \tag{18}$$

Considering the situation that only the distal phalanx is stressed. It is advisable to make the contact point between the distal phalanx and the object to be grasped as point D.

The rotation axis of the distal phalanx is the distal axis. The component force of the force at point F in the FC direction directly acts on the rotation axis of the distal phalanx, so this force does not affect the object being grasped. The force exerted on the object by the rotational moment generated after the force component of point F acting in the vertical direction of FC acts on the distal phalanx.

Under the action of the third spring and the second limit block, the proximal phalanx and the middle phalanx have not moved relatively. As a sequence, the quadrilateral AEFC maintains the parallelogram state, so the output torque of the second motor is transferred to the distal phalanx and directly acts on the object.

Combining the stress of these two parts, the force exerted on the object when contact with the distal phalanx is shown as follows:

$$\mathbf{F}_3 = \mathbf{R}_{z,-90^\circ} \cdot \left({\mathbf{F}_{F,\tau_1}}^T \cdot \left(\mathbf{R}_{z,90^\circ} \cdot \widehat{\mathbf{e}}_{FC} \right) \cdot \widehat{\mathbf{e}}_{CD} \right) \cdot l_4/l_3 + \tau_2/l_3 \cdot \mathbf{R}_{z,90^\circ} \cdot \widehat{\mathbf{e}}_{CD} \tag{19}$$

In order to facilitate the analysis of the middle self-adaptive grasping mode, it is assumed that points B and C is the contact point between the proximal and middle phalanx and the object, respectively. The force on the middle phalanx comes from the component force $\mathbf{F}_{FC}$ of the force at point F in the FC direction. The force perpendicular to the BC direction acts on the middle phalanx, and the pressure along the BC direction acts on the middle axis (point B).

To make the middle phalanx contact with the second limit block, the third spring has a pre-bending angle ξ_3. There is resistance from the third spring when the middle phalanx rotates relative to the proximal phalanx. The support force of the second limit block on the middle phalanx is offset by the resistance of the spring. Before the relative motion of the proximal and middle phalanxes, the proximal phalanx and the middle phalanx can be regarded as a whole. The force exerted by the proximal and middle phalanxes on the object is derived from the component of the force received at point C in the vertical direction of AC:

$$\mathbf{F}_2 = \left({\mathbf{F}_F}^T \cdot \widehat{\mathbf{e}}_{FC} \cdot \widehat{\mathbf{e}}_{FC} \right)^T \cdot \left(\mathbf{R}_{z,-90^\circ} \cdot \widehat{\mathbf{e}}_{BC} \right) \cdot \left(\mathbf{R}_{z,-90^\circ} \cdot \widehat{\mathbf{e}}_{BC} \right) \tag{20}$$

During middle phalanx self-adaptive grasping mode, the middle phalanx rotates angle α_2 relative to the proximal phalanx. Therefore, the exact contact force from the middle phalanx on the object is:

$$\mathbf{F}_{2,M-SA} = \left({\mathbf{F}_F}^T \cdot \widehat{\mathbf{e}}_{FC} \cdot \widehat{\mathbf{e}}_{FC} \right)^T \cdot \left(\mathbf{R}_{z,-90^\circ} \cdot \widehat{\mathbf{e}}_{BC} \right) \cdot \left(\mathbf{R}_{z,-90^\circ} \cdot \widehat{\mathbf{e}}_{BC} \right) - k_2(\alpha_2 + \xi_3)/l_2 \cdot \mathbf{R}_{z,-90^\circ} \cdot \widehat{\mathbf{e}}_{BC} \tag{21}$$

Lastly, consider the situation when only the proximal phalanx touches the object. Additionally, we will consider the middle phalanx self-adaptive grasping mode. Suppose point B is the contact point between the proximal phalanx and the object. The proximal phalanx, middle phalanx, and second spring are regarded as a whole, and the force exerted by the proximal phalanx on the object can be obtained as follows:

$$\mathbf{F}_1 = \left({\mathbf{F}_F}^T \cdot \widehat{\mathbf{e}}_{FC} \cdot \widehat{\mathbf{e}}_{FC} \right)^T \cdot \left(\mathbf{R}_{z,-90^\circ} \cdot \widehat{\mathbf{e}}_{AB} \right) \cdot \left(\mathbf{R}_{z,-90^\circ} \cdot \widehat{\mathbf{e}}_{AB} \right) \tag{22}$$

After the grasping mode is completed, the first and second pushing blocks rotate counterclockwise to make the first and second linkages return to the initial position through the first and second springs.

So far, given the input torque of the first and the second motor, the input force generated when the proximal, middle, and distal phalanx contacts the object at different positions has been solved.

3.2. Simulation

According to the derivation in Section 3.1, given the input torque and parameters in Table 2, we can obtain the force simulation when each phalanx of the MCG finger touches the object. The joint angle of the first linkage is obtained by the joint angle of the second linkage, middle phalanx, and middle phalanx. After re-arranging the joint angle, we can obtain the force of each phalanx in the x and y directions under the different joint angles of the first linkage and the second linkage.

Table 2. The parameters of the MCG finger.

Notation	Value	Unit
m_{1-7}	0.04, 0.04, 0.2, 0.03, 0.08, 0.07, 0.06	kg
l_{1-7}	0.040, 0.040, 0.035, 0.030, 0.080, 0.060, 0.050	m
ξ_{1-3}	$1/9 \cdot \pi$, $1/9 \cdot \pi$, $1/9 \cdot \pi$	rad
k_{1-3}	5, 5, 5	N/rad
β	$2/9 \cdot \pi$	rad
τ_{1-2}	1, 1	N·m

3.2.1. Simulation of the Proximal Phalanx

As shown in Figure 12, the force in the x-direction of the proximal phalanx has a peak when the joint angle of the first linkage is 30–40 degrees. This is because when the joint angle of the proximal phalanx is around 90 degrees, its component force in the horizontal direction is large. Correspondingly, the force in the y direction decreases with the increase in the joint angle. In the coupling grasping mode, such characteristics will help multiple fingers to grasp objects together.

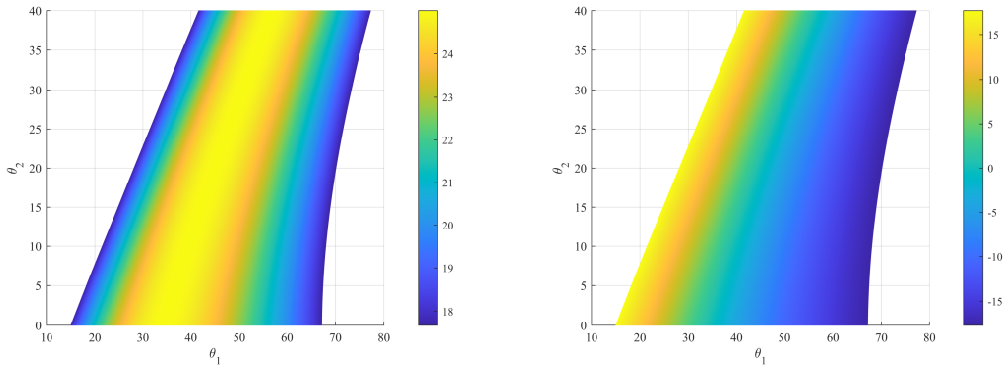

(**a**) (**b**)

Figure 12. Force simulation of the proximal phalanx (**a**) in x direction and (**b**) in y direction.

3.2.2. Simulation of the Middle Phalanx

The structure of the grasping force of the middle phalanx is the same as that of the proximal phalanx at different joint angles. Therefore, this section mainly analyzes the impact of the middle phalanx self-adaptive grasping mode.

As shown in Figure 13, the greater the rotation angle of the middle phalanx relative to the near phalanx, the smaller the force in the x and y directions. This is mainly because the middle phalanx needs to overcome the tension exerted by the third spring to maintain the attitude of the proximal and middle phalanxes during the M-SA mode. Therefore, within a specific angle range, the spring has a negligible impact on the grasping force, and the

adaptive middle finger is helpful for the enveloping grasping effect of the object. However, when the adaptive angle is too large, the resistance of the spring will excessively affect the grasping stability.

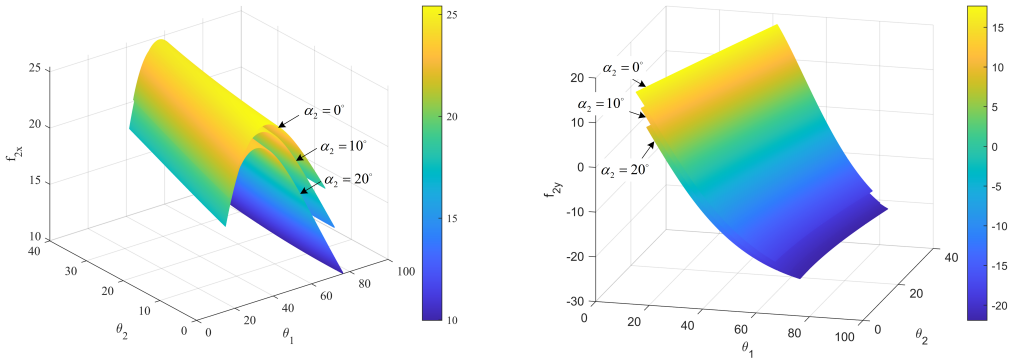

(**a**) (**b**)

Figure 13. Force simulation of the middle phalanx. (**a**) in x direction and (**b**) in y direction.

3.2.3. Simulation of the Distal Phalanx

The grasping force distribution of the distal phalanx reflects the characteristics under different grasping modes. As shown in Figure 14, the corresponding grasping modes of different angles have been marked.

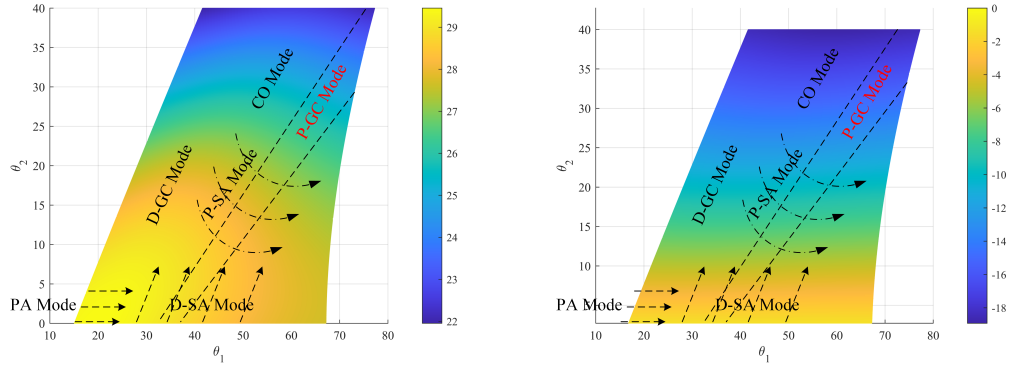

(**a**) (**b**)

Figure 14. Force simulation of the distal phalanx. (**a**) in x direction and (**b**) in y direction.

In the parallel grasping mode, the grasping force in the x-direction of the distal phalanx remains large and stable. In the coupling grasping mode, the component force in the y direction reaches the maximum value in the negative direction, which is consistent with its characteristics suitable for enveloping grasping. In the distal gesture changeable grasping mode, the component force in the y direction increases with the rotation of the distal phalanx, which is suitable for picking up objects. The proximal gesture changeable grasping mode is mainly responsible for the position switching, which is in the middle position in the distribution shown in Figure 14, and is helpful for the switching between various grasping modes.

3.3. Analysis of the Simulation Results

By synthesizing the mechanical analysis and simulation results of the three phalanxes, it can be concluded that the stress state of the MCG finger is stable in each grasping mode. In the prototype, we can control the first and second motors, respectively, according to the speed and state in Table 1, so as to control different grasping modes.

4. Prototype and Experiments

The prototype of the MCG finger has been manufactured and assembled, shown in Figure 15. The grasping experiments' results show that the MCG finger can finish the PA, CO, P-GC, D-GC, M-SA, and D-SA grasping modes and their combinations. The grasping experiment shows that the MCG finger has a good and stable grasping effect.

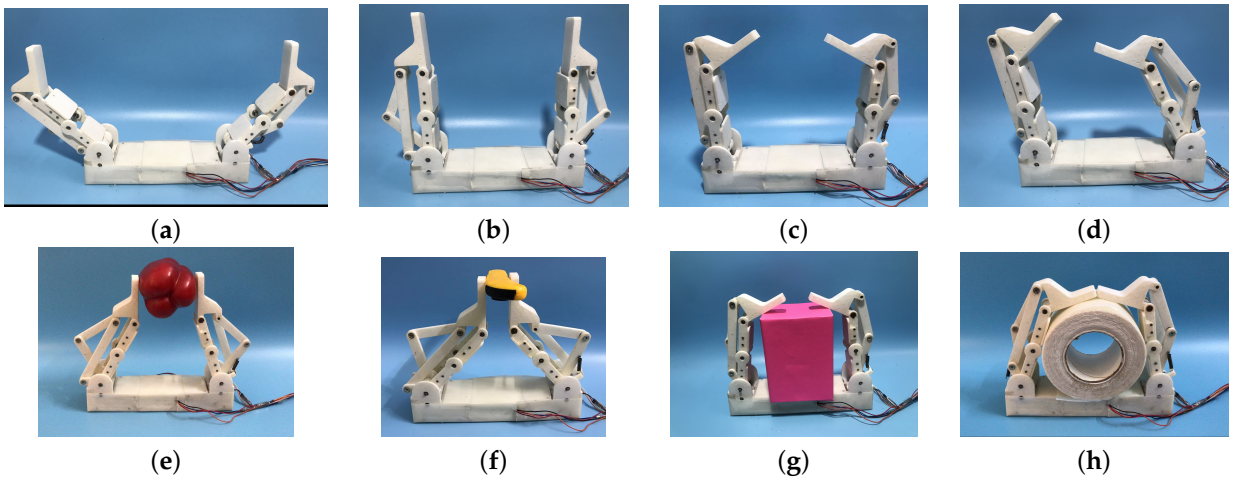

Figure 15. Grasping experiments of the MCG finger. (**a**) Initial state of parallel grasping mode, (**b**) Initial state of coupling grasping mode, (**c**) Gesture changeable grasping mode, (**d**) Coupling grasping mode, (**e**,**f**) paralleling grasping experiments, (**g**) Coupling grasping experiment, (**h**) Middle phalanx and distal phalanx self-adaptive grasping experiment.

5. Conclusions

The multi-mode compound grasping robot finger driven by linkage (MCG finger) is an innovative underactuated robot finger design that aims to address the challenges associated with dexterous hands, such as complex control systems and high costs. This paper proposes a new approach to robot finger design that integrates the flexibility of dexterous fingers with the simplicity of underactuated fingers. By adding a second actuator, the MCG finger is able to perform a variety of grasping modes, which makes it suitable for a wide range of applications.

The MCG finger has partially deviated from traditional underactuated hand design and is biased towards dexterous hand design. This means that it is able to offer the flexibility of a dexterous hand while still maintaining the simplicity of an underactuated mechanism. This is an important advantage of the MCG finger over other designs.

The paper introduces six grasping modes of the MCG finger and explains the structure and action modes of the finger. Theoretical analysis and prototype experiments are conducted to demonstrate the high grasping stability of the MCG finger under appropriate parameters.

In conclusion, the MCG finger represents a promising advancement in robotic finger design, providing a fresh approach to addressing the challenges associated with dexterous hands. With its range of grasping modes and the simplicity of its mechanism, the MCG finger lays the groundwork for future research into its potential applications and capabilities in numerous scientific and industrial settings.

Author Contributions: Conceptualization, Y.D. and W.Z.; Methodology, Y.D. and W.Z.; Validation, Y.D.; Formal analysis, Y.D.; Investigation, Y.D.; Resources, Y.D. and W.Z.; Data curation and W.Z., Y.D.; Writing—original draft, Y.D.; Writing—review & editing, Y.D. and W.Z.; Visualization, Y.D.; Supervision, W.Z.; Project administration, Y.D. All authors have read and agreed to the published version of the manuscript.

Funding: This research received no external funding.

Institutional Review Board Statement: Not applicable.

Informed Consent Statement: Not applicable.

Data Availability Statement: In the present article, the primary emphasis is placed on the design and simulation aspect of the study, with a comprehensive explanation of the simulation formulas delineated within the text. Consequently, no explicit code has been furnished for the derivation of the simulation data. It is important for readers to note that replicating the simulation outcomes can be achieved by accurately modeling the provided formulas. The data presented is solely based on the simulation formulas discussed in the manuscript.

Conflicts of Interest: The authors declare no conflict of interest.

Abbreviations

The following abbreviations are used in this manuscript:

MCG finger	Multi-mode compound grasping robot finger driven by linkage
CO mode	Coupling grasping mode
PA mode	Paralleling grasping mode
M-SA mode	Middle phalanx self-adaptive grasping mode
D-SA mode	Distal phalanx self-adaptive grasping mode
P-GC mode	Proximal gesture-changeable grasping mode
D-GC mode	Distal gesture-changeable grasping mode
COSA mode	Coupling and self-adaptive grasping mode
PASA mode	Paralleling and self-adaptive grasping mode
PA-M&D-SA mode	Paralleling and middle, distal phalanx composite grasping mode
CO-M&D-SA mode	Coupling and middle, distal phalanx composite grasping mode

References

1. Laffranchi, M.; Boccardo, N.; Traverso, S.; Lombardi, L.; Canepa, M.; Lince, A.; Semprini, M.; Saglia, J.A.; Naceri, A.; Sacchetti, R.; et al. The Hannes hand prosthesis replicates the key biological properties of the human hand. *Sci. Robot.* **2020**, *5*, eabb0467. [CrossRef] [PubMed]
2. Liu, M.J.; Xiong, C.H.; Xiong, L.; Huang, X.L. Biomechanical Characteristics of Hand Coordination in Grasping Activities of Daily Living. *PLoS ONE* **2016**, *11*, e0146193. [CrossRef] [PubMed]
3. Butterfass, J.; Hirzinger, G.; Knoch, S.; Liu, H. DLR's multisensory articulated hand. I. Hard- and software architecture. In Proceedings of the 1998 IEEE International Conference on Robotics and Automation (Cat. No.98CH36146), Leuven, Belgium, 20 May 1998; Volume 3, pp. 2081–2086. [CrossRef]
4. Butterfass, J.; Grebenstein, M.; Liu, H.; Hirzinger, G. DLR-Hand II: Next generation of a dextrous robot hand. In Proceedings of the 2001 ICRA. IEEE International Conference on Robotics and Automation (Cat. No.01CH37164), Seoul, Republic of Korea, 21–26 May 2001; Volume 1, pp. 109–114. [CrossRef]
5. Ramos, A.; Gravagne, I.; Walker, I. Goldfinger: A non-anthropomorphic, dextrous robot hand. In Proceedings of the 1999 IEEE International Conference on Robotics and Automation (Cat. No.99CH36288C), Detroit, MI, USA, 10–15 May 1999; Volume 2, pp. 913–919. [CrossRef]
6. Kawasaki, H.; Komatsu, T.; Uchiyama, K.; Kurimoto, T. Dexterous anthropomorphic robot hand with distributed tactile sensor: Gifu hand II. In Proceedings of the IEEE SMC'99 Conference Proceedings 1999 IEEE International Conference on Systems, Man, and Cybernetics (Cat. No.99CH37028), Tokyo, Japan, 12–15 October 1999; Volume 2, pp. 782–787. [CrossRef]
7. Kawasaki, H.; Komatsu, T.; Uchiyama, K. Dexterous anthropomorphic robot hand with distributed tactile sensor: Gifu hand II. *IEEE/ASME Trans. Mechatron.* **2002**, *7*, 296–303. [CrossRef]
8. Meghdari, A.; Sayyaadi, H. Optimization in Trajectory Planning of Multi-Jointed Fingers in Dextrous Hand Designs. In Proceedings of the International Design Engineering Technical Conferences and Computers and Information in Engineering Conference, Santa Clara, CA, USA, 18–22 August 1991; Volume 2—Finite Elements/Computational Geometry; Computers in Education; Robotics and Controls; pp. 496–502. [CrossRef]
9. Birglen, L.; Laliberté, T.; Gosselin, C.M. *Underactuated Robotic Hands*; Springer: Berlin, Germany, 2007; Volume 40.
10. Laliberté, T.; Gosselin, C.M. Simulation and design of underactuated mechanical hands. *Mech. Mach. Theory* **1998**, *33*, 39–57. [CrossRef]
11. Laliberte, T.; Birglen, L.; Gosselin, C. Underactuation in robotic grasping hands. *Mach. Intell. Robot. Control* **2002**, *4*, 1–11.
12. Dollar, A.M.; Howe, R.D. Joint coupling design of underactuated grippers. In Proceedings of the International Design Engineering Technical Conferences and Computers and Information in Engineering Conference, Philadelphia, PA, USA, 10–13 September 2006; Volume 42568, pp. 903–911.

13. Bencak, P.; Hercog, D.; Lerher, T. Simulation Model for Robotic Pick-Point Evaluation for 2-F Robotic Gripper. *Appl. Sci.* **2023**, *13*, 2599. [CrossRef]
14. Ma, R.R.; Odhner, L.U.; Dollar, A.M. A modular, open-source 3D printed underactuated hand. In Proceedings of the 2013 IEEE International Conference on Robotics and Automation, Karlsruhe, Germany, 6–10 May 2013; pp. 2737–2743. [CrossRef]
15. Dollar, A.M.; Howe, R.D. The SDM Hand as a Prosthetic Terminal Device: A Feasibility Study. In Proceedings of the 2007 IEEE 10th International Conference on Rehabilitation Robotics, Noordwijk, The Netherlands, 13–15 June 2007; pp. 978–983. [CrossRef]
16. Pollayil, G.J.; Pollayil, M.J.; Catalano, M.G.; Bicchi, A.; Grioli, G. Sequential contact-based adaptive grasping for robotic hands. *Int. J. Robot. Res.* **2022**, *41*, 543–570. [CrossRef]
17. Ilievski, F.; Mazzeo, A.D.; Shepherd, R.F.; Chen, X.; Whitesides, G.M. Soft robotics for chemists. *Angew. Chem.* **2011**, *123*, 1930–1935. [CrossRef]
18. Deimel, R.; Brock, O. A novel type of compliant and underactuated robotic hand for dexterous grasping. *Int. J. Robot. Res.* **2016**, *35*, 161–185. [CrossRef]
19. Hussain, I.; Malvezzi, M.; Gan, D.; Iqbal, Z.; Seneviratne, L.; Prattichizzo, D.; Renda, F. Compliant gripper design, prototyping, and modeling using screw theory formulation. *Int. J. Robot. Res.* **2021**, *40*, 55–71. [CrossRef]
20. Ciocarlie, M.T.; Allen, P.K. Hand posture subspaces for dexterous robotic grasping. *Int. J. Robot. Res.* **2009**, *28*, 851–867. [CrossRef]
21. Matrone, G.C.; Cipriani, C.; Carrozza, M.C.; Magenes, G. Real-time myoelectric control of a multi-fingered hand prosthesis using principal components analysis. *J. Neuroeng. Rehabil.* **2012**, *9*, 1–13. [CrossRef] [PubMed]
22. Ji, D.; Lee, J.; Jin, M. Design and control of hybrid Flexible robotic gripper with high stiffness and stability. In Proceedings of the 2022 13th Asian Control Conference (ASCC), Jeju, Republic of Korea, 4–7 May 2022; pp. 2503–2505. [CrossRef]
23. Della Santina, C.; Grioli, G.; Catalano, M.; Brando, A.; Bicchi, A. Dexterity augmentation on a synergistic hand: The Pisa/IIT SoftHand+. In Proceedings of the 2015 IEEE-RAS 15th International Conference on Humanoid Robots (Humanoids), Seoul, Republic of Korea, 3–5 November 2015; pp. 497–503.
24. Tincani, V.; Catalano, M.G.; Farnioli, E.; Garabini, M.; Grioli, G.; Fantoni, G.; Bicchi, A. Velvet fingers: A dexterous gripper with active surfaces. In Proceedings of the 2012 IEEE/RSJ International Conference on Intelligent Robots and Systems, Vilamoura-Algarve, Portugal, 7–12 October 2012; pp. 1257–1263. [CrossRef]
25. Ruan, S.; Zhang, W.; Zhang, T.; Song, S. COSA-FBA hand: An underactuated hand with five-gear mechanisms and built-in actuators. In *Mechanism and Machine Science*; Springer: Berlin, Germany, 2016; pp. 121–130.
26. Dang, L.; Song, J.; Wei, Y.; Zhang, W. COSA-LET finger: A novel coupled and self-adaptive robot finger with a linear empty-trip transmission. In Proceedings of the 2017 2nd International Conference on Advanced Robotics and Mechatronics (ICARM), Hefei, China, 27–31 August 2017; pp. 334–338. [CrossRef]
27. Sun, J.; Zhang, W. COSA finger: A coupled and self-adaptive under-actuated unit for humanoid robotic hand. In *International Conference on Social Robotics*; Springer: Berlin, Germany, 2010; pp. 172–181.
28. Hang, K.; Li, M.; Stork, J.A.; Bekiroglu, Y.; Pokorny, F.T.; Billard, A.; Kragic, D. Hierarchical fingertip space: A unified framework for grasp planning and in-hand grasp adaptation. *IEEE Trans. Robot.* **2016**, *32*, 960–972. [CrossRef]
29. Ko, T. A tendon-driven robot gripper with passively switchable underactuated surface and its physics simulation based parameter optimization. *IEEE Robot. Autom. Lett.* **2020**, *5*, 5002–5009. [CrossRef]
30. Yang, Y.; Xu, X.; Zhang, W. A parallel and self-adaptive underactuated finger with novel belt and cam-link mechanisms. In Proceedings of the 2016 International Conference on Advanced Robotics and Mechatronics (ICARM), Macau, China, 18–20 August 2016; pp. 635–639. [CrossRef]
31. Ciocarlie, M.; Hicks, F.M.; Holmberg, R.; Hawke, J.; Schlicht, M.; Gee, J.; Stanford, S.; Bahadur, R. The Velo gripper: A versatile single-actuator design for enveloping, parallel and fingertip grasps. *Int. J. Robot. Res.* **2014**, *33*, 753–767. [CrossRef]
32. Fantoni, G.; Santochi, M.; Dini, G.; Tracht, K.; Scholz-Reiter, B.; Fleischer, J.; Lien, T.K.; Seliger, G.; Reinhart, G.; Franke, J.; et al. Grasping devices and methods in automated production processes. *CIRP Ann.* **2014**, *63*, 679–701. [CrossRef]
33. Che, D.; Zhang, W. Active gesture-changeable underactuated finger for humanoid robot hand based on multiple tendons. *Mech. Sci.* **2010**, *1*, 27–32. [CrossRef]
34. Luo, T.; Zhang, W.; Liu, H. A novel coupled gesture-changeable under-actuated robotic finger with linkage and gear-rack mechanism. In Proceedings of the 2010 IEEE International Conference on Robotics and Biomimetics, Tianjin, China, 14–18 December 2010; pp. 1093–1097. [CrossRef]
35. Weyrich, M.; Abdullah, M.W. Concept of a three D.O.F spherical-joint gripper for industrial robots. In Proceedings of the 2013 IEEE 18th Conference on Emerging Technologies & Factory Automation (ETFA), Cagliari, Italy, 10–13 September 2013; pp. 1–4. [CrossRef]
36. Heung, K.H.; Tong, R.K.; Lau, A.T.; Li, Z. Robotic glove with soft-elastic composite actuators for assisting activities of daily living. *Soft Robot.* **2019**, *6*, 289–304. [CrossRef] [PubMed]
37. Yoshida, K.; Yamada, H.; Kato, R.; Seki, T.; Yokoi, H.; Mukai, M. Development of five-finger robotic hand using master-slave control for hand-assisted laparoscopic surgery. In Proceedings of the 2016 38th Annual International Conference of the IEEE Engineering in Medicine and Biology Society (EMBC), Orlando, FL, USA, 16–20 August 2016; pp. 5124–5127. [CrossRef]
38. Hashira, I.; Kato, R.; Ishizaka, K. Development of a Humanoid Hand System to Support Robotic Urological Surgery. In Proceedings of the 2022 44th Annual International Conference of the IEEE Engineering in Medicine & Biology Society (EMBC), Glasgow, UK, 11–15 July 2022; pp. 4849–4852. [CrossRef]

39. Sapaty, P. Military robotics: Latest trends and spatial grasp solutions. *Int. J. Adv. Res. Artif. Intell.* **2015**, *4*, 9–18.
40. Samadikhoshkho, Z.; Zareinia, K.; Janabi-Sharifi, F. A brief review on robotic grippers classifications. In Proceedings of the 2019 IEEE Canadian Conference of Electrical and Computer Engineering (CCECE), Edmonton, AB, Canada, 5–8 May 2019; pp. 1–4.
41. Prattichizzo, D.; Trinkle, J.C. Grasping. In *Springer Handbook of Robotics*; Springer: Berlin, Germany, 2016; pp. 955–988.